nature catalysis

Article

https://doi.org/10.1038/s41929-023-01065-5

Enantioselective decarboxylative alkylation using synergistic photoenzymatic catalysis

Received: 30 May 2023

Accepted: 20 October 2023

Published online: 18 December 2023

Check for updates

Shang-Zheng Sun[1], Bryce T. Nicholls[1], David Bain[1], Tianzhang Qiao[1], Claire G. Page[1], Andrew J. Musser[1] & Todd K. Hyster[2]

Photoenzymatic catalysts are attractive for stereoselective radical reactions because the transformation occurs within tunable enzyme active sites. When using flavoproteins for non-natural photoenzymatic reactions, reductive mechanisms are often used for radical initiation. Oxidative mechanisms for radical formation would enable abundant functional groups, such as amines and carboxylic acids, to serve as radical precursors. However, excited state flavin is short-lived in many proteins because of rapid quenching by the protein scaffold. Here we report that adding an exogenous $Ru(bpy)_3^{2+}$ cofactor to flavin-dependent 'ene'-reductases enables the redox-neutral decarboxylative coupling of amino acids with vinylpyridines with high yield and enantioselectivity. Additionally, stereo-complementary enzymes are found to provide access to both enantiomers of the product. Mechanistic studies indicate that $Ru(bpy)_3^{2+}$ binds to the protein, helping to localize radical formation to the enzyme's active site. This work expands the types of transformation that can be rendered asymmetric using photoenzymatic catalysis and provides an intriguing mechanism of radical initiation.

Enzymes catalyse a litany of unique and selective transformations to facilitate essential reactions for life[1]. The polypeptide scaffold is frequently the target of optimization because its primary sequence can be modified using various mutagenesis techniques[2,3]. However, cofactors bound by the protein are often responsible for the bond-forming events in a reaction[4–7]. As researchers have explored whether naturally occurring enzymes can catalyse non-natural reactions, the reactivity available to the cofactor has become central to hypothesis-driven studies[8–12]. Flavin is a versatile cofactor with access to different mechanisms based on its oxidation state[13,14]. Over the past six years, our group and others have demonstrated that flavin hydroquinone (FMN_{hq}) and flavin semiquinone (FMN_{sq}), either in their ground or excited states, can initiate radical reactions via single electron reduction of substrates within the active sites of 'ene'-reductases (EREDs)[15–19] and Baeyer–Villiger monooxygenases (BVMOs)[20]. In general, enzymes are tolerant of high reduction potentials because they lack easily reduced functionality. Moreover, as radical formation occurs via enzyme-templated charge transfer complexes, the electron transfer events are localized and minimize the formation of reactive radical species, which could degrade the protein.

Oxidative radical formation represents a significant challenge for photoenzymes because the excited state of flavin can be quenched by oxidizing amino acid side chains (such as tyrosines or tryptophans), making it challenging to use this state for productive chemistry[21]. Fatty acid photodecarboxylase (FAP) is the only known flavoprotein to use its excited state to oxidatively generate substrate-centred radicals[22]. This enzyme has a long-lived excited state and is fluorescent because there are few tyrosines and tryptophans proximal to the flavin cofactor (Y156 8.55 Å, Y466 8.62 Å)[23]. However, this protein is currently limited to hydrodecarboxylation reactions[24–26]. We sought to develop a strategy that would enable catalytically promiscuous EREDs to utilize oxidative mechanisms for radical formation as it would allow ubiquitous moieties, such as carboxylic acids and amines, to serve as radical precursors for intermolecular reactions[27,28].

Reductive quenching by the protein scaffold accounts for the short-lived excited state (24 ps) of FMN in old yellow enzyme 1 (OYE1)[29]. Consequently, rather than relying on FMN for substrate oxidation, we considered adding an exogenous photo-oxidant to initiate radical formation within the protein active site. As this oxidizing cofactor

[1]Department of Chemistry and Chemical Biology, Cornell University, Ithaca, NY, USA. [2]Present address: Department of Chemistry, Princeton University, Princeton, NJ, USA. e-mail: thyster@princeton.edu

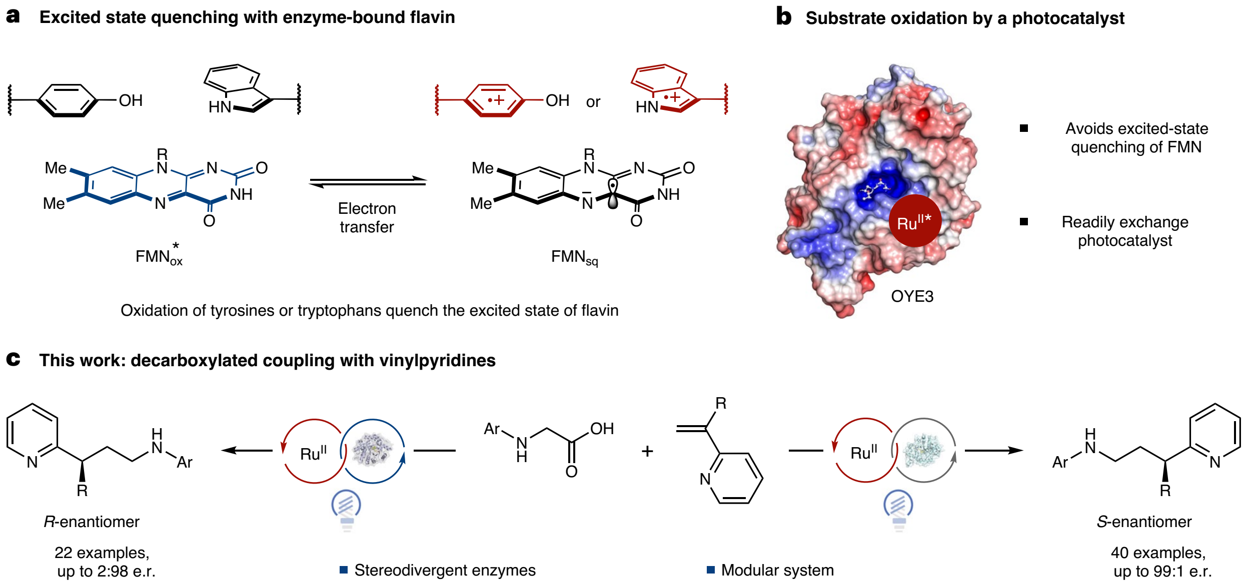

Fig. 1 | Strategies for photoenzymatic oxidative radical formation for an intermolecular coupling reaction. a, The excited state of flavin can be quenched by oxidizing amino acid residues, such as tyrosines and tryptophans. **b**, Strategy for oxidative radical generation via photoenzymatic catalysis. **c**, Enantiodivergent decarboxylative alkylation using synergistic photoenzymatic catalysis.

would not be localized within a protein active site rich with tyrosines and tryptophans, the excited state could be sufficiently long-lived to enable substrate oxidation. We previously demonstrated that exogenous photocatalysts could reduce substrates within ERED sites[30,31]. In these systems, the protein can activate the substrate for reduction by serving as a hydrogen-bond donor, making reduction within the active site thermodynamically favoured. However, this type of mechanism is ineffective for controlling oxidative radical formation. We set out to develop a synergistic approach for oxidative radical formation in the hope that a selective reaction would reveal a new control mechanism that could be broadly applied to oxidative radical formation within proteins. In this Article, we report an enantiodivergent decarboxylative alkylation of amino acids with vinylpyridines and demonstrate up to 92% yield and 99:1 enantiomeric ratio (e.r.) by adding an exogenous $Ru(bpy)_3^{2+}$ cofactor to flavin-dependent EREDs. Mechanistic studies indicate that $Ru(bpy)_3^{2+}$ binds to the protein, which localizes radical formation to the enzyme's active site (Fig. 1).

Results and discussion

Reaction development

We initiated our studies by exploring the redox-neutral coupling of *N*-phenyl glycine **1a** with vinylpyridine **2a** (Fig. 2). This reaction involves the generation of a nucleophilic radical, an intermediate with different reactivity to electrophilic radicals currently used by EREDs. It affords a chiral product containing a pyridine ring, which is a common motif in pharmaceuticals[32]. While this type of transformation was previously rendered asymmetric using chiral phosphoric acids, we envisioned a biocatalytic variant as a proving ground for an alternative photoenzymatic radical initiation mechanism[33,34]. In a previous study, we demonstrated that combining the ERED from *Nostoc punctiforme* (NostocER) with $Ru(bpy)_3Cl_2$ as a photo-reductant enabled the asymmetric reduction of vinylpyridines[35]. When using the same reaction conditions but for the proposed decarboxylative coupling, we observed the desired product in 83% yield with 80:20 e.r. Building on this result, we tested a series of ERED homologues and ultimately found that old yellow enzyme 3 (OYE3) formed product in 90% yield with 93:7 e.r., favouring the *S*-enantiomer. During this screen, we also found that GluER-T36A, the enzyme we often used for reductive coupling reactions, afforded product in 70:30 e.r., favouring the

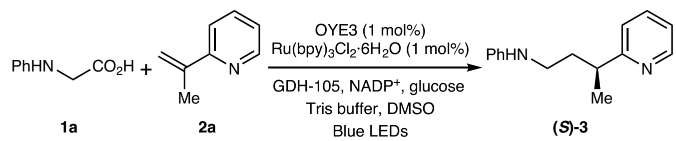

Entry[a,b]	Enzyme screen	Yield (%)	e.r.
1	NostocER	83	80:20
2	OYE3	90	93:7
3	GluER-T36A	68	30:70
4[c]	GluER-T36A-Y343D	44	11:89
	Variation from reaction with OYE3		
5	No OYE3	70	50:50
6	No $Ru(bpy)_3Cl_2$	3	97:3
7	No GDH-105, $NADP^+$, glucose	78	76:24
8	No $Ru(bpy)_3Cl_2$, GDH-105, $NADP^+$, glucose	2	65:35
9	No OYE3, GDH-105, $NADP^+$, glucose	51	50:50
10	No light	0	–

Fig. 2 | Optimization of enantioselective decarboxylative alkylation. [a]Reaction conditions: *N*-phenylglycine (**1a**, 10 μmol, 1 equiv.), 2-(prop-1-en-2-yl)pyridine (**2a**, 35 μmol, 3.5 equiv.), purified OYE3 (1 mol%), $Ru(bpy)_3Cl_2 \cdot 6H_2O$ (1 mol%), $NADP^+$ (1 mol%), GDH-105 (0.3 mg ml^{-1}) and glucose (1.5 equiv.) in Tris buffer (900 μl, 100 mM, pH 7.6), with DMSO (150 μl, 14% v/v) as co-solvent. The final total volume was 1,050 μl. Reaction mixtures were irradiated with blue light-emitting diodes (LEDs) under anaerobic conditions at room temperature for 14 h. [b]Yield (average of duplicate measurements) determined using liquid chromatography–mass spectrometry relative to an internal standard 1,3,5-tribromobenzene (TBB). e.r. (*S*:*R*) determined by high-performance liquid chromatography on a chiral stationary phase. [c]Tricine buffer (100 mM, pH 9.0), 16 h.

R-enantiomer. Testing previously compiled mutants, we found that GluER-T36A-Y343D improved the enantioselectivity to 89:11 e.r. with 44% yield. A test of different photocatalysts with both enzymes failed to enhance the yields or enantioselectivities. Control experiments confirmed essential features of this reaction. When OYE3 is removed, the coupling reaction occurs in 71% yield but as a racemate, indicating that the photocatalyst can facilitate radical initiation and termination without the protein. By contrast, when the photocatalyst is removed, the product is formed in 2% yield but with 97:3 e.r., suggesting that the protein is responsible for radical termination. The reduced enantioselectivity observed when the cofactor turnover mix is removed (65:35 e.r.) is likely due to radical termination from FMN_{sq} rather than FMN_{hq}. As FMN_{sq} has a weaker N5–H bond (59.5 kcal mol^{-1}) than FMN_{hq} (79.3 kcal mol^{-1})[36], radical termination should have an earlier transition state resulting in reduced enantioselectivity. Consequently, it is essential to add a cofactor regeneration system to ensure that reactions initiate with FMN in the hydroquinone oxidation state. Moreover, to avoid a racemic background reaction, the loading of $Ru(bpy)_3Cl_2$ needs to be precisely controlled (1:1 ratio with OYE3).

Mechanistic investigations

With a selective reaction, we were interested in understanding how high enantioselectivity is achieved despite the potential for a significant racemic background reaction. Our initial hypothesis was that ERED activated the substrate for oxidation via a proton-coupled electron transfer mechanism. If this were the case, we would expect the reaction to be accelerated by the presence of the protein because the first irreversible step is oxidative decarboxylation. To our surprise, nearly identical rates were observed with and without protein, suggesting that the protein is not accelerating carboxylic acid oxidation (Supplementary Fig. 28). This is further supported by Stern–Volmer quenching studies, which indicate that *N*-phenylglycine quenches Ru(II)* with a quenching rate constant of $K_q = 41.4\ M^{-1}\ s^{-1}$ (Fig. 3a). When reduced OYE3 is added to the same quenching experiments, a negligible change in the quenching constant is observed, confirming that the protein does not accelerate substrate oxidation (Supplementary Fig. 21).

Having ruled out enzyme activation of the substrate for oxidation, we considered that radical formation and C–C bond formation occurs in solution to form a persistent or dynamically stable radical selectively terminated within the protein active site. We conducted a density functional theory (DFT) calculation to probe this possibility to determine the strength of the C–C bond formed upon radical dimerization. We calculate the bond strength as 35.4 kcal mol^{-1} (Fig. 3b). While weaker than a prototypical C–C bond (80 kcal mol^{-1}), it is too strong to form reversibly, indicating that radical generation and C–C bond formation are not occurring in solution[37].

Our final hypothesis was that radical formation occurs within the protein active site because of an association between the photocatalyst and the protein. This association would ensure that radical formation occurs near the enzyme's active site, helping to favour termination within the active site rather than in solution. To probe this possibility, we conducted fluorescence-quenching experiments. OYE3 is a steady-state quencher of the $Ru(bpy)_3^{2+}$ excited state. When time-resolved fluorescence quenching was conducted, we did not observe quenching, indicating a static quenching mechanism where $Ru(bpy)_3^{2+}$ associates with OYE3 (refs. 38,39). Based on the quencher concentration, we calculate a K_D of 7.94 μM. This indicates a strong association between the enzyme and the cofactor, providing a mechanism for localizing radical formation near the protein (Fig. 3c). While the exact location of association is unknown, previous studies by Wilson and co-workers suggest that $Ru(bpy)_3^{2+}$ and structural analogues tend to reside in hydrophobic pockets on the protein surface[39]. Examining an electrostatic map of OYE3 reveals possible hydrophobic pockets flanking the flavin binding site where the photocatalyst could bind.

We propose the following mechanism based on the association between the photocatalyst and enzyme (Fig. 3e). Initially, the ERED is reduced from FMN_{ox} (flavin quinone) to FMN_{hq} using the cofactor turnover mix. Next, the *N*-phenylglycine and the vinylpyridine bind to the protein active site. Excitation of $Ru(bpy)_3^{2+}$ affords an excited state that oxidizes the carboxylate to afford an α-amino radical and $Ru(bpy)_3^{1+}$. To determine whether the photocatalyst oxidizes the amine or carboxylate, we tested *N*-[(trimethylsilyl)methyl]aniline (**1b,** E_{ox} = +0.53 versus standard calomel electrode (SCE)) (Supplementary Fig. 29)[40]. This coupling partner provides the model product **3** in 76% yield with similar enantioselectivity to that observed with the carboxylic acid, suggesting that the radical initiation is most likely to occur through amine oxidation. This α-amino radical can react with the vinylpyridine to afford a benzylic radical. Experiments with a vinylpyridine containing a cyclopropane group show formation of the ring-opened product, suggesting that C–C bond formation occurs via a radical mechanism (Supplementary Fig. 32). The use of α-trifluoromethylstyrene shows coupled product formation with only 1% yield of defluorination product **6**, indicating that the radical termination occurs via hydrogen atom transfer (Fig. 3d). Deuterium incorporation experiments were conducted to determine the source of the hydrogen atom. However, the results of these studies were inconclusive, presumably due to washing out of the isotopic label[41] (Supplementary Fig. 34). We reasoned that only the O–H bond of tyrosine or the N5–H bond of flavin were sufficiently weak to serve as hydrogen-atom donors. When variants where prepared where active site tyrosines were mutated to phenylalanine (OYE3-Y83F, OYE3-Y197F and OYE3-Y376F) and subjected to the standard reaction conditions, only modest changes in enantioselectivity were observed, suggesting that none were serving as hydrogen-atom donors (Supplementary Fig. 39). Based on these results, the modest level of deuterium incorporation when using D_2O buffer and the importance of the cofactor turnover, we hypothesize that FMN_{hq} is responsible for radical termination. The resulting FMN_{sq} can oxidize $Ru(bpy)_3^{1+}$ via electron transfer followed by protonation to regenerate FMN_{hq} and $Ru(bpy)_3^{2+}$. Based on this proposed mechanism, the cofactor turnover mix should not be necessary. Indeed, when the cofactor turnover mix is replaced with 1 mol% NADPH, the desired product is formed in 64% yield and 86:14 e.r. (Supplementary Fig. 5). We attribute the lower yields to competitive quenching of $[Ru(bpy)_3^{2+}]^*$ by $NADP^+$ (Supplementary Fig. 22).

Substrate scope of the enantiodivergent decarboxylative alkylation

Encouraged by these initial findings, we began investigating the generality of our enantioselective decarboxylative alkylation of amino acids with α-heterocyclic olefins (Fig. 4). Various alkenes with *ortho*, *meta* and *para* substituents on the pyridine ring were efficiently converted into cross-coupled products in good yields and with good levels of enantioselectivity (**3, 7**–**17**). Beyond 2-pyridines, this system also accommodates pyrimidines (to give **18**), pyrazines (to give **19** and **20**), thiazoles (to give **25** and **26**), 3-pyridines (to give **21**) and 4-pyridines (to give **22**), yielding the desired products in good yield and excellent stereoselectivity (up to 99:1 e.r. and 2:98 e.r., respectively). However, OYE3 was limited to small functional groups at the α-position of the olefins, either slightly large heterocycles (to give **23** and **24**) or alkyl groups (to give **27**–**29**), decreasing the stereoselectivity. We anticipated that protein engineering could be applied to improve the stereoselectivity in some cases. We note that a heteroaromatic alkene (to give **30**) and acrylamide (to give **32**) were equally tolerated, favouring decarboxylative cross-coupling rather than direct reduction by EREDs under photoredox conditions[35,42]. This highlights the excellent chemoselectivity of our decarboxylative alkylation technology. Also tolerated are 1,2-disubstituted olefins (to give **31**), albeit with more modest selectivity. Notably, this reaction could occur with 1.0 mmol, affording (*S*)-**3** in 70% yield without reduction in enantioselectivity.

Next, we evaluated the influence of the amino acid precursors on the catalytic decarboxylative alkylation event. As expected, the substituents on the phenyl ring of the *N*-arylglycine were largely inconsequential to the reactivity profile (products **33**–**40**).

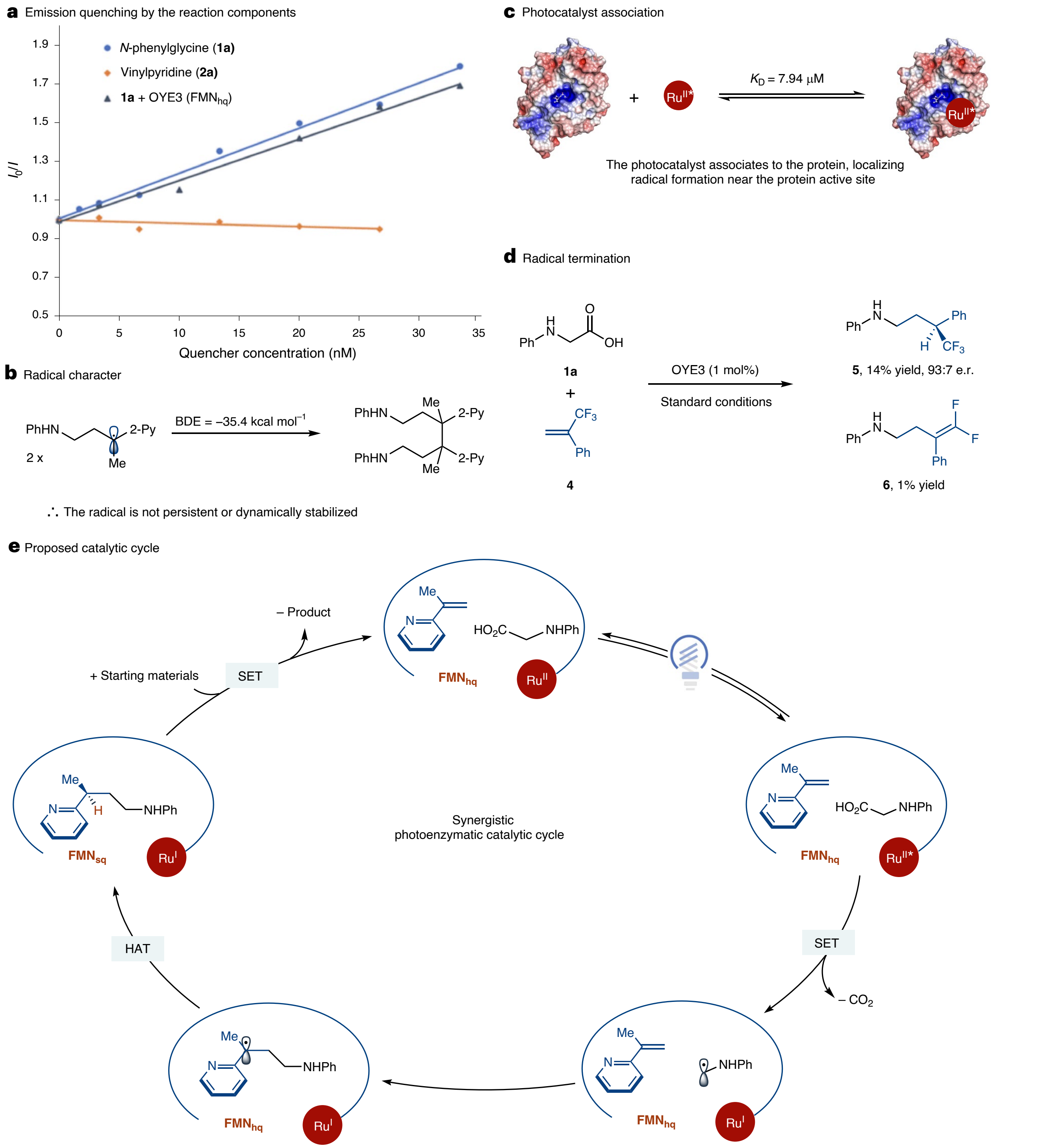

Fig. 3 | Mechanistic studies and proposed catalytic cycle. a, A Stern–Volmer quenching study indicates that *N*-phenylglycine quenches Ru(II)* and the protein (OYE3) does not accelerate substrate oxidation. **b**, DFT calculation to determine the strength of the C–C bond formed upon radical dimerization. 2-Py, 2-pyridine. **c**, Binding assay study of Ru(bpy)$_3$Cl$_2$ and OYE3, suggesting a strong association between Ru(bpy)$_3^{2+}$ and OYE3 (K_D = 7.94 μM). **d**, A radical termination study indicates that radical termination occurs via hydrogen atom transfer from FMN$_{hq}$ rather than stepwise reduction and protonation. **e**, Proposed catalytic cycle. SET, single electron transfer; HAT, hydrogen atom transfer.

In addition, secondary *N*-phenyl phenylalanine (to give **41**) and indoline-2-carboxylic acid (to give **42**) underwent targeted reaction in good yields and with good e.r. values but no diastereoselectivity. This indicates that the stereoselectivity is controlled by the hydrogen-atom transfer step rather than the C–C bond-formation step. A more sterically encumbered tertiary carboxylic acid could be converted into **43** with moderate enantioselectivity.

Aiming to explore our method's synthetic applicability, an *anti*-human cytomegalovirus (HCMV) compound **47** was synthesized in three steps from 8-aminoquinoline in moderate yield and with good enantioselectivity[43] (Fig. 5). Driven by the advantage of the excellent chemo- and enantio-selectivity of this ERED and photoredox dual catalytic event, we wondered whether the more electronically activated olefins can be applied in the reaction. As shown, methyl

https://doi.org/10.1038/s41929-023-01065-5

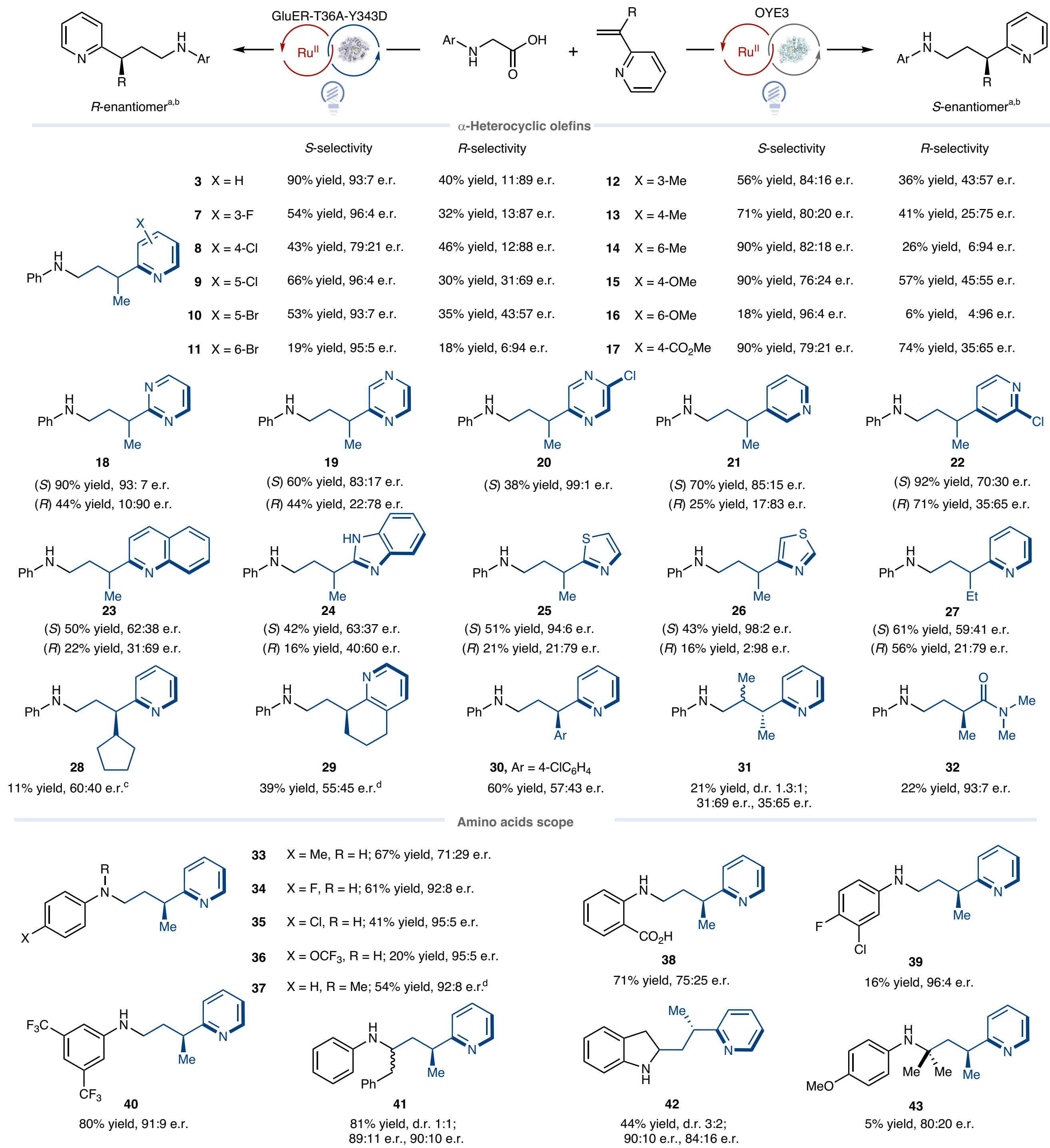

Fig. 4 | Scope of the enantioselective decarboxylative alkylation. Reaction conditions for providing (***S***)-enantiomers: amino acids (10 µmol, 1 equiv.), α-olefins (35 µmol, 3.5 equiv.), purified OYE3 (1 mol%), $Ru(bpy)_3Cl_2{\cdot}6H_2O$ (1 mol%), $NADP^+$ (1 mol%), GDH-105 (0.3 mg ml^{-1}) and glucose (1.5 equiv.) in Tris buffer (900 µl,100 mM, pH 7.6), with DMSO (150 µl, 14% v/v) as co-solvent. The final total volume was 1,050 µl. Reaction mixtures were irradiated with blue light-emitting diodes (LEDs) under anaerobic conditions at room temperature for 14 h. Reaction conditions for providing (*R*)-enantiomers: amino acids (10 µmol, 1 equiv.), α-olefins (35 µmol, 3.5 equiv.), purified GluER-T36A-Y343D (1 mol%), $Ru(bpy)_3Cl_2{\cdot}6H_2O$ (1 mol%), $NADP^+$ (1 mol%), GDH-105 (0.3 mg ml^{-1}) and glucose (1.5 equiv.) in tricine (900 µl, 100 mM, pH 9.0), with DMSO (150 µl, 14% v/v) as co-solvent. The final total volume was 1,050 µl. Reaction mixtures were irradiated with blue LEDs under anaerobic conditions at room temperature for 16 h. [a]Yields (average of two separate reactions, determined using liquid chromatography–mass spectrometry relative to an internal standard TBB. e.r. refers to the ratio of (*S*)- to (*R*)-enantiomers, determined by high-performance liquid chromatography on a chiral stationary phase. [b]Isolated yields are given for a 0.10 mmol-scale reaction: **3** (84% yield, 93:7 e.r.), **9** (58% yield, 96:4 e.r.), **17** (56% yield, 79:21 e.r.), **18** (68% yield, 93:7 e.r.), **20** (34% yield, 99:1 e.r.), **21** (66% yield, 85:15 e.r.), **25** (46% yield, 94:6 e.r.), **34** (74% yield, 92:8 e.r.), **39** (18% yield, 96:4 e.r.), **41** (70% yield, 1:1 diastereomeric ratio (d.r.), 89:11 e.r., 90:10 e.r.). [c]Tris buffer (900 µl,100 mM, pH 9.0), with DMSO (150 µl, 14% v/v) as co-solvent. The final total volume was 1,050 µl. [d]Without $NADP^+$, GDH-105 and glucose.

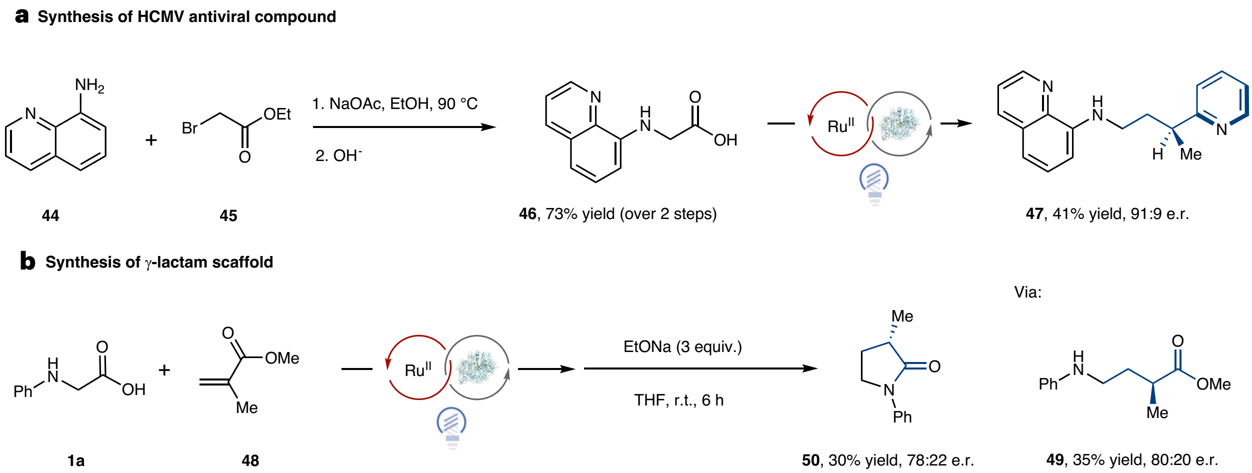

Fig. 5 | Synthetic application. a, Synthesis of HCMV antiviral compound **47** using OYE3, NaOAc, sodium acetate; EtOH, ethanol. **b**, Synthesis of γ-lactam **50** using OYE3 (EtONa, sodium ethoxide).

methacrylate (**48**) was subjected to the reaction, followed by treatment with sodium ethoxide (3.0 equiv.), affording γ-lactam **50** with moderate enantioselectivity.

Conclusion

In conclusion, we have established an enantiodivergent decarboxylative alkylation of amino acids with α-heterocyclic olefins through the synergistic merger of EREDs and photoredox catalysis. This protocol is distinguished by its excellent chemo- and enantio-selectivity and broad scope. Overall, this synergetic approach provides an intriguing mechanism for radical generation and expands the types of reaction that can be rendered asymmetric using non-natural enzymatic catalysis.

Methods

Protein expression and purification

Saccharomyces cerevisiae old yellow enzymes (OYE3s) were expressed in *Escherichia coli* BL21 (DE3) after transformation with a plasmid containing the gene for OYE3. Transformed glycerol stocks were used to initiate a 5 ml overnight culture in Luria–Bertani (LB) media with ampicillin (100 µg ml^{-1}) at a temperature of 37 °C and with stirring at 250 r.p.m. Turbo Broth media (500 ml in a 2 l baffled shake flask) containing ampicillin (100 µg ml^{-1}) and auto-inducing mixture were inoculated with 2 ml of the overnight culture and then grown at a temperature of 30 °C and with stirring at 250 r.p.m. for 24 h. The cells were harvested by centrifugation (4,000*g*, 20 min, 4 °C). Cell pellets were resuspended in purification binding buffer at a concentration of 1 g cell pellet per 1 ml binding buffer, transferred to 50 ml conical centrifuge tubes, frozen and stored at −20 °C.

Purification. Cell pellets were thawed in cool water. Enzymatic lysis was initiated by adding lysozyme (1 mg ml^{-1}), DNase I (0.1 mg ml^{-1}), FMN (1 mg ml^{-1}) and phenylmethylsulfonyl fluoride (PMSF, 1 mM). Enzymatic lysis was performed for 30 min with shaking at 37 °C. Cells were further disrupted by sonication, then the lysates were centrifuged (20,000*g*, 1.5 h, 4 °C). Proteins were purified using a nickel-NTA column. Untagged proteins were washed off the column with binding buffer A (50 mM TEOA, pH 7.0, 300 mM NaCl, 25 mM imidazole) over 15 column volumes. Enzymes were eluted with elution buffer B (50 mM TEOA, pH 7.0, 300 mM NaCl, 250 mM imidazole) over five column volumes. Yellow fractions containing OYE3 enzymes were pooled, concentrated using 10 kDa spin concentrators and subjected to three buffer exchanges into an imidazole free storage buffer C (50 mM TEOA, pH 7.0). Concentrated enzymes (1–4 mM) were aliquoted to 100 nmol fractions, flash frozen in liquid nitrogen and stored at −80 °C until later use.

General procedure for providing the *S*-enantiomers

To a 4 ml reaction vial charged with a stir bar, an amino acid (**1**, 10 µmol, 1.0 equiv.) and glucose (2.7 mg, 1.5 equiv.) were added. Then the vial was transferred into a Coy anaerobic chamber. In the Coy anaerobic chamber, $Ru(bpy)_3Cl_2{\cdot}6H_2O$ (0.064 mg, 1 mol%, 100 µl, 0.64 mg ml^{-1} stock solution in dimethylsulfoxide (DMSO), $NADP^+$ (1 mol%) and GDH-105 stock solution [50 µl, $NADP^+$ (3 mg) and GDH (12 mg) were dissolved in 2 ml Tris buffer (100 mM, pH 7.6)], an olefin (**2**, 35 µmol, 3.5 equiv.), Tris buffer (850 µl, 100 mM, pH 7.6) and DMSO (50 µl, total volume was 150 µl, 14% v/v) were added separately using a pipette. The reaction total volume was 1,050 µl. Subsequently, purified OYE3 (1.0 mol%) was added using a pipette. The vial was sealed with a rubber cap and removed from the anaerobic chamber. Reaction mixtures were irradiated with blue light-emitting diodes and stirred (200 r.p.m.) for 14 h while under fan cooling.

General procedure for providing the *R*-enantiomers

To a 4 ml reaction vial charged with a stir bar, an amino acid (**1**, 10 µmol, 1.0 equiv.) and glucose (2.7 mg, 1.5 equiv.) were added. Then the vial was transferred into a Coy anaerobic chamber. In the Coy anaerobic chamber, $Ru(bpy)_3Cl_2{\cdot}6H_2O$ (0.064 mg, 1 mol%, 100 µl, 0.64 mg ml^{-1} stock solution in DMSO), $NADP^+$ (1 mol%) and GDH-105 stock solution [50 µl, $NADP^+$ (3 mg) and GDH (12 mg) were dissolved in 2 ml tricine buffer (100 mM, pH 9.0)], an olefin (**2**, 35 µmol, 3.5 equiv.), tricine buffer (850 µl, 100 mM, pH 9.0) and DMSO (50 µl, total volume was 150 µl, 14% v/v) were added separately using a pipette. The reaction total volume was 1,050 µl. Subsequently, purified GluER-T36A-Y343D (1.0 mol%) was added using a pipette. The vial was sealed with a rubber cap and removed from the anaerobic chamber. Reaction mixtures were irradiated with blue light-emitting diodes and stirred (200 r.p.m.) for 16 h while under fan cooling.

Reporting summary

Further information on research design is available in the Nature Portfolio Reporting Summary linked to this article.

Data availability

The data that support the findings in this study are available within the paper and its Supplementary Information or from the corresponding author upon reasonable request.

References

1. Bornscheuer, U. T. et al. Engineering the third wave of biocatalysis. *Nature* **485**, 185–194 (2012).
2. Bell, E. L. et al. Biocatalysis. *Nat. Rev. Methods Primers* **1**, 46 (2021).
3. Reetz, M. T. & Carballeira, J. D. Iterative saturation mutagenesis (ISM) for rapid directed evolution of functional enzymes. *Nat. Protoc.* **2**, 891–903 (2007).
4. Begley, T. P. Cofactor biosynthesis: an organic chemist's treasure trove. *Nat. Prod. Rep.* **23**, 15–25 (2006).
5. Richter, M. Functional diversity of organic molecule enzyme cofactors. *Nat. Prod. Rep.* **30**, 1324–1345 (2013).
6. Barra, L., Awakawa, T. & Abe, I. Noncanonical functions of enzyme cofactors as building blocks in natural product biosynthesis. *JACS Au* **2**, 1950–1963 (2022).
7. Prier, C. K. & Arnold, F. H. Chemomimetic biocatalysis: exploiting the synthetic potential of cofactor-dependent enzymes to create new catalysts. *J. Am. Chem. Soc.* **137**, 13992–14006 (2015).
8. Jeschek, M. et al. Directed evolution of artificial metalloenzymes for *in vivo* metathesis. *Nature* **537**, 661–665 (2016).
9. Chen, K. & Arnold, F. H. Engineering new catalytic activities in enzymes. *Nat. Catal.* **3**, 203–213 (2020).
10. Emmanuel, M. A., Greenberg, N. R., Oblinsky, D. G. & Hyster, T. K. Accessing non-natural reactivity by irradiating nicotinamide-dependent enzymes with light. *Nature* **540**, 414–417 (2016).
11. Zhou, Q., Chin, M., Fu, Y., Liu, P. & Yang, Y. Stereodivergent atom-transfer radical cyclization by engineered cytochromes P450. *Science* **374**, 1612–1616 (2021).
12. Rui, J. et al. Directed evolution of nonheme iron enzymes to access a biological radical-relay C(sp^3)–H azidation. *Science* **376**, 869–874 (2022).
13. Massey, V. Introduction: flavoprotein structure and mechanism. *FASEB J.* **9**, 473–475 (1995).
14. Walsh, C. T. & Wencewicz, T. A. Flavoenzymes: versatile catalysts in biosynthetic pathways. *Nat. Prod. Rep.* **30**, 175–200 (2013).
15. Biegasiewicz, K. F. et al. Photoexcitation of flavoenzymes enables a stereoselective radical cyclization. *Science* **364**, 1166–1169 (2019).
16. Black, M. J. et al. Asymmetric redox-neutral radical cyclization catalyzed by flavin-dependent 'ene'-reductases. *Nat. Chem.* **12**, 71–75 (2020).
17. Fu, H. et al. Ground-state electron transfer as an initiation mechanism for biocatalytic C–C bond forming reactions. *J. Am. Chem. Soc.* **143**, 9622–9629 (2021).
18. Fu, H. et al. An asymmetric sp^3–sp^3 cross-electrophile coupling using biocatalysis. *Nature* **610**, 302–307 (2022).
19. Huang, X. et al. Photoenzymatic enantioselective intermolecular radical hydroalkylation. *Nature* **584**, 69–74 (2020).
20. Peng, Y. et al. Photoinduced promiscuity of cyclohexanone monooxygenase for the enantioselective synthesis of α-fluoroketones. *Angew. Chem. Int. Ed.* **61**, e202211199 (2022).
21. Munro, A. W. & Noble, M. A. in *Flavoprotein Protocols. Methods in Molecular Biology* Vol. 131, 25–48 (eds Chapman, S. K. & Reid, G. A.) (Humana Press, 1999).
22. Moulin, S. L. Y. et al. Fatty acid photodecarboxylase is an ancient photoenzyme that forms hydrocarbons in the thylakoids of algae. *Plant Physiol.* **186**, 1455–1472 (2021).
23. Zhang, B., Liebl, U. & Vos, M. H. Flavoprotein photochemistry: fundamental processes and photocatalytic perspectives. *J. Phys. Chem. B* **126**, 3199–3207 (2022).
24. Sorigué, D. et al. An algal photoenzyme converts fatty acids to hydrocarbons. *Science* **357**, 903–907 (2017).
25. Zhang, W. et al. Hydrocarbon synthesis via photoenzymatic decarboxylation of carboxylic acids. *J. Am. Chem. Soc.* **141**, 3116–3120 (2019).
26. Xu, J. et al. Light-driven decarboxylative deuteration enabled by a divergently engineered photodecarboxylase. *Nat. Commun.* **12**, 3983 (2021).
27. Nakajima, K., Miyake, Y. & Nishibayashi, Y. Synthetic utilization of α-aminoalkyl radicals and related species in visible light photoredox catalysis. *Acc. Chem. Res.* **49**, 1946–1956 (2016).
28. Beil, S. B., Chen, T. Q., Intermaggio, N. E. & MacMillan, D. W. C. Carboxylic acids as adaptive functional groups in metallaphotoredox catalysis. *Acc. Chem. Res.* **55**, 3481–3494 (2022).
29. Kudisch, B. et al. Active-site environmental factors customize the photophysics of photoenzymatic old yellow enzymes. *J. Phys. Chem. B* **124**, 11236–11249 (2020).
30. Biegasiewicz, K. F., Cooper, S. J., Emmanuel, M. A., Miller, D. C. & Hyster, T. K. Catalytic promiscuity enabled by photoredox catalysis in nicotinamide-dependent oxidoreductases. *Nat. Chem.* **10**, 770–775 (2018).
31. Ye, Y. et al. Using enzymes to tame nitrogen-centred radicals for enantioselective hydroamination. *Nat. Chem.* **15**, 206–212 (2022).
32. Ling, Y. et al. The expanding role of pyridine and dihydropyridine scaffolds in drug design. *Drug Des. Dev. Ther.* **15**, 4289–4338 (2021).
33. Yin, Y. et al. Conjugate addition enantioselective protonation of *N*-aryl glycines to α-branched 2-vinylazaarenes via cooperative photoredox and asymmetric catalysis. *J. Am. Chem. Soc.* **140**, 6083–6087 (2018).
34. Yin, Y. et al. All-carbon quaternary stereocenters α to azaarenes via radical-based asymmetric olefin difunctionalization. *J. Am. Chem. Soc.* **142**, 19451–19456 (2020).
35. Nakano, Y. et al. Photoenzymatic hydrogenation of heteroaromatic olefins using 'ene'-reductases with photoredox catalysts. *Angew. Chem. Int. Ed.* **59**, 10484–10488 (2020).
36. Warren, J. J., Tronic, T. A. & Mayer, J. M. Thermochemistry of proton-coupled electron transfer reagents and its implications. *Chem. Rev.* **110**, 6961–7001 (2012).
37. Sakamaki, D., Ghosh, S. & Seki, S. Dynamic covalent bonds: approaches from stable radical species. *Mater. Chem. Front.* **3**, 2270–2282 (2019).
38. Hewitt, S. H. et al. Protein surface mimetics: understanding how ruthenium tris(bipyridines) interact with proteins. *ChemBioChem* **18**, 223–231 (2017).
39. Filby, M. H. et al. Protein surface recognition using geometrically pure Ru(II) tris(bipyridine) derivatives. *Chem. Commun.* **47**, 559–561 (2011).
40. Espelt, L. R., McPherson, I. S., Wiensch, E. M. & Yoon, T. P. Enantioselective conjugate additions of α-amino radicals via cooperative photoredox and Lewis acid catalysis. *J. Am. Chem. Soc.* **137**, 2452–2455 (2015).
41. Sandoval, B. A. et al. Photoenzymatic catalysis enables radical-mediated ketone reduction in ene-reductases. *Angew. Chem. Int. Ed.* **58**, 8714–8718 (2019).
42. Sandoval, B. A. et al. Photoenzymatic reductions enabled by direct excitation of flavin-dependent 'ene'-reductases. *J. Am. Chem. Soc.* **143**, 1735–1739 (2021).
43. Remiszevski, S., Koyuncu, E., Sun, Q. & Chiang, L. Anti-hcmv compositions and methods. WO patent 2016077240A2 (2016).

Acknowledgements

We thank the S. Lin, P. Milner, A. Musser and R. A. Cerione groups for use of their equipment and the D. Collum group for use of their computational resources. S.-Z.S. thanks Z. Lu (S. Lin group) for helping with electrochemical measurements and W. Fu (SJTU) for examining the electrostatic map of OYE3. S.-Z.S. thanks H. Fu and Y. Ye for discussion. The research reported here was supported by https://doi.org/10.1038/s41929-023-01065-5

the National Science Foundation CHE-2135973. C.G.P. acknowledges the NSF-GFRP for support. This work made use of the Cornell University NMR Facility, which is supported, in part, by the NSF though MRI Award CHE-1531632.

Author contributions

T.K.H. conceived and directed the project. S.-Z.S. and T.K.H. designed the experiments. S.-Z.S. and B.T.N. performed experiments and analysed the results. T.Q. conducted DFT experiments. D.B. and A.J.M. conducted and analysed time-resolved fluorescence spectroscopy. C.G.P helped with revisions of the manuscript. The manuscript was prepared with feedback from all the authors.

Competing interests

The authors declare no competing interests.

Additional information

Supplementary information The online version contains supplementary material available at https://doi.org/10.1038/s41929-023-01065-5.

Correspondence and requests for materials should be addressed to Todd K. Hyster.

Peer review information *Nature Catalysis* thanks Qi Wu and the other, anonymous, reviewer(s) for their contribution to the peer review of this work.

nature research

Corresponding author(s): Hyster, Todd K.

Reporting Summary

Nature Research wishes to improve the reproducibility of the work that we publish. This form provides structure for consistency and transparency in reporting. For further information on Nature Research policies, see Authors & Referees and the Editorial Policy Checklist.

Statistical parameters

When statistical analyses are reported, confirm that the following items are present in the relevant location (e.g. figure legend, table legend, main text, or Methods section).

n/a	Confirmed	
☐	☒	The exact sample size (*n*) for each experimental group/condition, given as a discrete number and unit of measurement
☒	☐	An indication of whether measurements were taken from distinct samples or whether the same sample was measured repeatedly
☒	☐	The statistical test(s) used AND whether they are one- or two-sided *Only common tests should be described solely by name; describe more complex techniques in the Methods section.*
☒	☐	A description of all covariates tested
☒	☐	A description of any assumptions or corrections, such as tests of normality and adjustment for multiple comparisons
☐	☒	A full description of the statistics including central tendency (e.g. means) or other basic estimates (e.g. regression coefficient) AND variation (e.g. standard deviation) or associated estimates of uncertainty (e.g. confidence intervals)
☒	☐	For null hypothesis testing, the test statistic (e.g. *F*, *t*, *r*) with confidence intervals, effect sizes, degrees of freedom and *P* value noted *Give P values as exact values whenever suitable.*
☒	☐	For Bayesian analysis, information on the choice of priors and Markov chain Monte Carlo settings
☒	☐	For hierarchical and complex designs, identification of the appropriate level for tests and full reporting of outcomes
☒	☐	Estimates of effect sizes (e.g. Cohen's *d*, Pearson's *r*), indicating how they were calculated
☒	☐	Clearly defined error bars *State explicitly what error bars represent (e.g. SD, SE, CI)*

Our web collection on statistics for biologists may be useful.

Software and code

Policy information about availability of computer code

Data collection	A Spectrapro HRS300 spectrometer (150 g/mm) and PI-MAX4 ICCD camera were used time-resolved photoluminescence and photoluminescence quantum yield for detection. All DFT computations were carried out using guassian 15 revision C.01 program and the B3LYP-D3(BJ) functional. The contiuum solvation model of densities (SMD) has been employed. Structures were optimized at the B4LYP-D3(BJ) level of theory. Higher level of theory single point calculations used SMD in water were carried out on B3LYP-D3(BJ)/def2TZVP. The surface charge of enzyme was caluclated using the APCS plugin in PyMOL.
Data analysis	Yield of enzymatic reactions were determinted by LCMS based on standard curve using 1,3,5-tribromobenzene (TBB) as internal standard . Chiral HPLC was conducted using an Agilent 1260 Infinity chiral HPLC system with isopropanol and hexanes as the mobile phase. Chiral IA, IB, IC, OD, AS-H and OJ-H columns were used to separate enantiomers (4.6 x 20 mm, 5 µm) at room temperature. 1H- and 13C-NMR spectra were recorded on Bruker (400 MHz and 101 MHz, respectively) and Bruker (500 MHz and 126 MHz, respectively) instrument with deuterated chloroform or dimethyl sulfoxide-d6 as solvents as noted. 19F-NMR spectra were recorded on a Bruker 400 (376 MHz) instruments.

For manuscripts utilizing custom algorithms or software that are central to the research but not yet described in published literature, software must be made available to editors/reviewers upon request. We strongly encourage code deposition in a community repository (e.g. GitHub). See the Nature Research guidelines for submitting code & software for further information.

Data

Policy information about availability of data

All manuscripts must include a data availability statement. This statement should provide the following information, where applicable:

- Accession codes, unique identifiers, or web links for publicly available datasets
- A list of figures that have associated raw data
- A description of any restrictions on data availability

All data are available in the main text or the supplementary materials

Field-specific reporting

Please select the best fit for your research. If you are not sure, read the appropriate sections before making your selection.

☒ Life sciences ☐ Behavioural & social sciences ☐ Ecological, evolutionary & environmental sciences

For a reference copy of the document with all sections, see nature.com/authors/policies/ReportingSummary-flat.pdf

Life sciences study design

All studies must disclose on these points even when the disclosure is negative.

Sample size	Scope investigations were conducted at 10 umol scale and analyzed via LCMS. Substrates 9, 17, 18, 20, 21, 25, 34, 39, and 41 were performed at 0.1 mmol scale and product yields were determined via isolation. Substrates 3 wasperformed at 1.0 mmol scale with isolated yield reported.
Data exclusions	No date was excluded
Replication	All enzymatic reactions were repeated at least twice. All attempts at replication were successful.
Randomization	NA. No group allocation involved in this study.
Blinding	NA. No group allocation involved in this study.

Reporting for specific materials, systems and methods

Materials & experimental systems

n/a	Involved in the study
☐	☒ Unique biological materials
☒	☐ Antibodies
☒	☐ Eukaryotic cell lines
☒	☐ Palaeontology
☒	☐ Animals and other organisms
☒	☐ Human research participants

Methods

n/a	Involved in the study
☒	☐ ChIP-seq
☒	☐ Flow cytometry
☒	☐ MRI-based neuroimaging

Unique biological materials

Policy information about availability of materials

Obtaining unique materials	Genes encoding the enzymes were codon optimized and purchased from a dna synthesis company and cloned into commercial expression vectors.